CRS-attribute-based residual static correction

I. Koglin and E. Ewig

email: *Ingo.Koglin@gpi.uni-karlsruhe.de*

keywords: *residual static correction, CRS moveout*

ABSTRACT

Residual static correction methods are usually applied to onshore data sets, as these data sets are influenced by the inhomogeneity of the uppermost low-velocity layer, the so-called weathering layer. Thus, residual static correction methods are used to eliminate the influence on reflection traveltimes due to the weathering layer and/or any errors introduced by redatuming methods. Their aim is to enhance the results of stacking methods applied after residual static correction, which should show an improved signal-to-noise ratio. As the Common-Reflection-Surface stack provides additional information beyond conventional stacking velocities about the subsurface in the form of kinematic wavefield attributes, we considered to make use of it. These attributes define a stacking surface within a spatial aperture rather than a curve within the common-midpoint gathers, only. With the knowledge of the attributes, the Common-Reflection-Surface operator can be corrected for its moveout which is mandatory for the determination of residual statics. Our method presented in the following is based on cross correlations. Furthermore, the moveout corrected traces and pilot traces are normalized before the cross correlation. Our method for residual static correction was applied to a real data example.

INTRODUCTION

Onshore real data sets usually suffer from the influence of topography and the uppermost low-velocity layer, the so-called weathering layer. Therefore, statics are used to eliminate these influences. On the one hand, the topographic effect on the reflection times can be significantly reduced by applying so-called field or elevation statics. On the other hand, the effects of rapid changes in elevation and in near-surface velocity or thickness of the weathering layer still remain as reflection time distortions. Therefore, residual static correction methods are applied to compensate these remains. The residual static correction tries to eliminate these remains by assigning every source and every receiver location an additional static time shift. These time shifts of residual static corrections aim at enhancing the continuity of the reflection events and at improving the signal-to-noise (S/N) ratio after stacking.

The 2D zero-offset (ZO) Common-Reflection-Surface (CRS) stack method has shown its abilities to improve the S/N ratio under the assumption of a horizontal plane measurement surface (see Trappe et al., 2001). Zhang (2003) has introduced the topography into the CRS stack method. This can be seen as a more sophisticated kind of field static correction and its results can also serve as input for our residual static correction method. As stacking methods in general, the 2D ZO CRS stack method does not directly account for residual static corrections. Similar to the conventional common-midpoint (CMP) based methods, a new alternative approach for residual static correction based on the CRS attributes is presented in the following.

BASICS OF STATIC CORRECTIONS

The main assumption for applying static corrections is surface consistency. This implies that the waves propagate nearly vertical through the uppermost layer and, hence, independently from the raypaths in the deeper layers (see Figure 1(b)). Thus, the time shifts become properties of the source or receiver locations, only. Furthermore, the reflection time distortions do not depend on the traveltime of different reflection

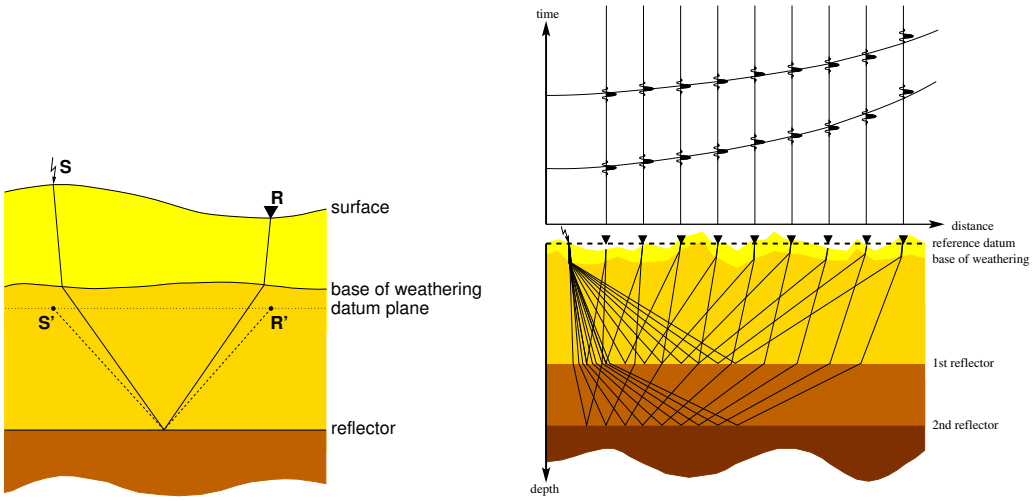

Figure 1: (a) Raypath through a low-velocity layer. Redatuming achieved by field static correction substitutes the actual surface by a reference datum plane beneath the low-velocity layer, i. e., source S and receiver R are moved to S' and R' on the reference datum plane, respectively. (b) illustrates the possible influence of the weathering layer on the traces. Additionally, two possible stacking operators are displayed in the upper part.

events, i. e., they are reflection time independent. Therefore, these time shifts are called static corrections. Another assumption is that the weathering layer has the same influence on the shape of the wavelet for all emerging reflection events. The latter assumption is due to the fact that we do not account for phase shifts of the wavelet at the moment.

Under these assumptions, static corrections can be divided into two parts:

- The field or elevation static correction, which is a kind of redatuming, introduces a reference datum plane as substitute for the actual measurement surface. This reference datum is mostly located beneath the weathering layer (see Figure 1(a)). For further explanations, please refer to Marsden (1993).
- The residual static correction is used to eliminate small variations of reflection traveltimes caused by the weathering layer. Additionally, errors from redatuming by field static correction or other methods can be removed. Even though, residual static correction can be also applied without any preceeding static correction to enhance the imaging quality.

Conventional residual static correction methods

To achieve surface consistency, residual static correction techniques have to provide exactly one time shift for every source or receiver location, respectively. The first step of most of the conventional residual static correction techniques is to apply an approximate normal moveout (NMO) correction. Then, the reflection events in each CMP gather are considered to be misaligned due to a source static, a receiver static, a residual moveout, and additional terms depending on the used method. The calculated time shifts t_{ij} of each trace consist of the following terms

$$t_{ij} = t_{r_i} + t_{s_j} + M_k X_{ij}^2 + \ldots \quad \text{with} \quad k = \frac{i+j}{2}\,, \tag{1}$$

where t_{r_i} is the receiver static of the i-th receiver location and t_{s_j} is the source static for the j-th source location. M_k is the residual moveout at the k-th CMP gather and $X_{ij} = r_i - s_j$ is the source to receiver

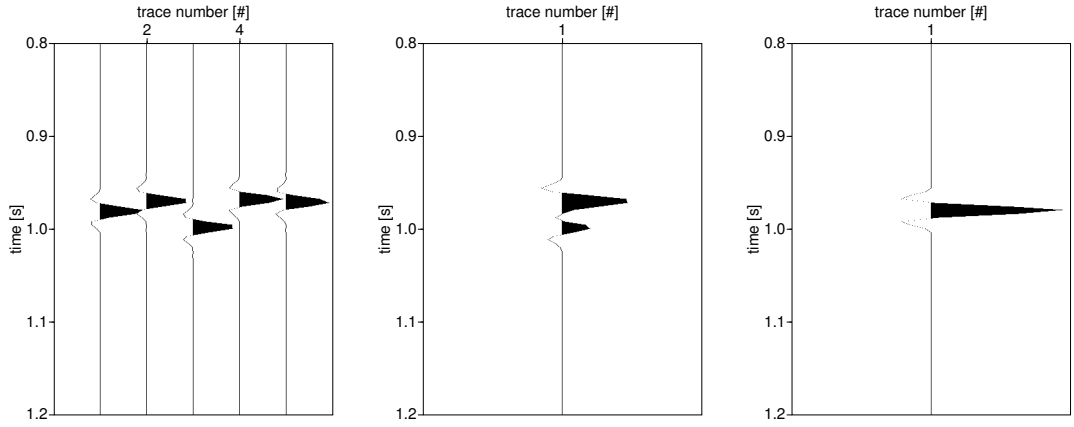

(a) synthetic gather

(b) stacked 'as is'

(c) stacked after residual static correction

Figure 2: Example of the enhancement due to residual static correction after an approximate NMO correction.

distance, i. e., the offset (see Taner et al., 1974; Wiggins et al., 1976; Cox, 1974) between the source location s_j and the receiver location r_i. Figure 2 shows an example of the improvements of the stacking result due to residual static correction. Figure 2(a) shows a reflection event after NMO correction, distorted by residual statics. Stacking these traces without any corrections results in a deformed wavelet (see Figure 2(b)), while the stack with residual static correction clearly yields a well preserved wavelet with larger amplitudes due to the coherent stack (see Figure 2(c)).

From this point on, many different conventional methods exist to determine t_{ij} or t_{r_i} and t_{s_j}, respectively. One method, e. g., is to cross correlate all traces of each CMP gather with their corresponding CMP stacked trace which is used as pilot trace for this CMP gather. The window for the correlation has to be selected to cover more than one dominant primary event (time invariance) and at reasonably large traveltimes (surface consistency). Thus, a system of equations of t_{ij} is given by one equation for each trace of the whole data set. This large system of linear equations is overdetermined, i. e., there are more equations than unknowns, and underconstrained, i. e., there are more unknowns than independent equations. The solution is generally obtained by least-square techniques.

Ronen and Claerbout (1985) introduced another technique for residual static correction based on cross correlation, the stack power maximization method. Here, the cross correlation is performed between so-called super-traces. A super-trace built from all the traces of the shot profile in sequence (trace F in Figure 3) is cross correlated with another super-trace analogously built of all traces in the relevant part of the stack without the contribution of that shot (trace G in Figure 3). The source static of this shot is the time associated with the global maximum of the cross correlation result. This procedure is repeated for every shot and receiver profile, respectively. The resulting time shifts maximize the sum of squared amplitudes of the final stack, i. e., the stack power.

RESIDUAL STATIC CORRECTION BY MEANS OF CRS ATTRIBUTES

In addition to the simulated ZO section, the CRS stack method provides three further sections with CRS attributes. These attributes (α, R_{NIP}, R_{N}) are parameters of the second-order stacking surface given by

$$t_{hyp}^2(x,h) = \left[t_0 + \frac{2}{v_0}(x-x_0)\sin\alpha\right]^2 + \frac{2}{v_0}t_0\cos^2\alpha\left[\frac{(x-x_0)^2}{R_{\mathrm{N}}} + \frac{h^2}{R_{\mathrm{NIP}}}\right], \qquad (2)$$

with the ZO traveltime t_0, the near-surface velocity v_0, the emergence angle α of the ZO ray, the radius of curvature of the NIP wavefront R_{NIP} measured at x_0, and the radius of curvature of the normal wavefront

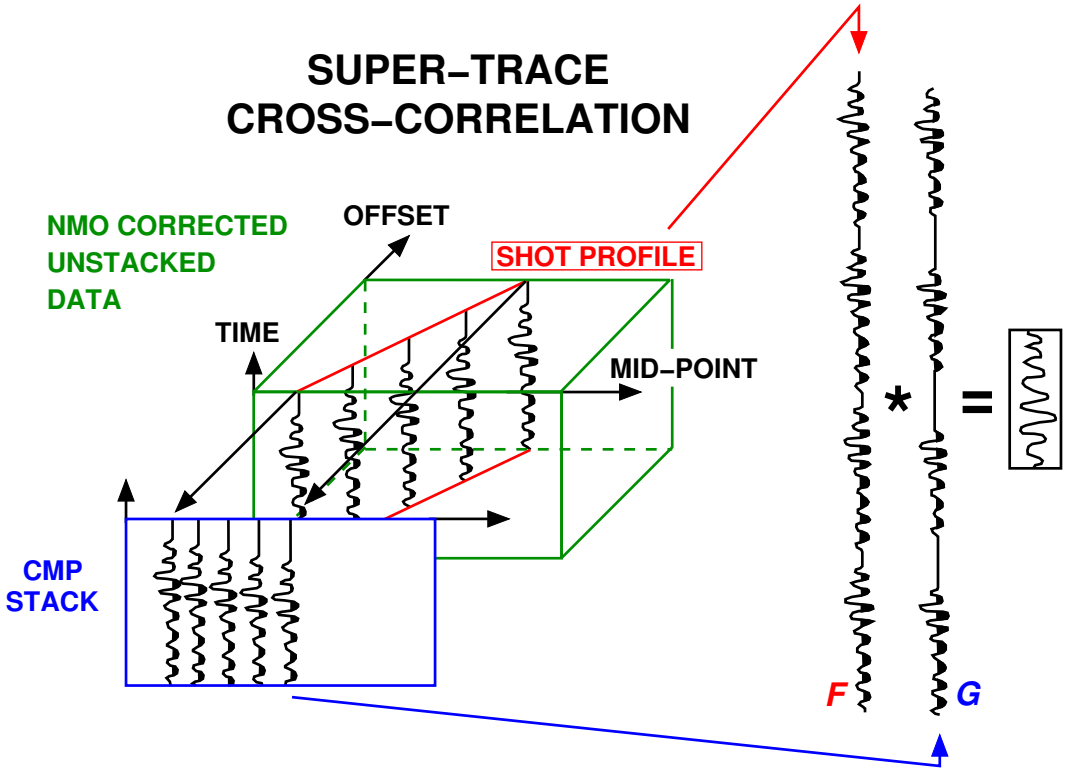

Figure 3: Example of super-traces for one moveout corrected shot gather. Super-trace F and super-trace G are cross correlated to determine the corresponding source static. Figure taken from Ronen and Claerbout (1985).

R_{N} also measured at x_0 (see, e. g., Mann et al., 1999, for these definitions). This stacking surface from the CRS stack method improves the S/N ratio more than, e. g., the NMO/DMO/stack method due to the larger stacking surface (see Mann, 2002; Trappe et al., 2001).

Our new approach is also based on cross correlations and is similar to the technique of Ronen and Claerbout (1985). Figure 4 shows the principal steps of our method. The first step is to perform at least the initial 2D ZO CRS stack to obtain the CRS attribute sections and the simulated ZO section. Each trace of the simulated ZO section serves as a pilot trace for the necessary cross correlations. Additionally, the optimized 2D ZO CRS stack can also be used for the subsequent steps. However, this requires more processing time due to a local optimization of the attributes. The initial CRS stack differs from the optimized one by the strategy to obtain the attributes. The attributes of the initial search serve as starting values for the optimized search. Irrespectively of how the attributes are obtained, the CRS moveout correction is then realized with the previously obtained CRS attributes.

CRS moveout correction

To correct for the CRS moveout, the dependency on the half-offset h and the midpoint x in equation (2) has to be eliminated. Therefore, the CRS attributes of every time sample within the simulated ZO section are required. These attributes are provided by the initial or optimized search of the CRS stack method. With the knowledge of these attributes, the Common-Reflection-Surface can be transformed into a horizontal plane at time t_0 by subtracting the moveout given by

$$t_{moveout}(x,h) = t_{hyp}(x,h) - t_0\,, \tag{3}$$

where t_0 is given by the considered time sample of the simulated ZO section (see Figure 5).

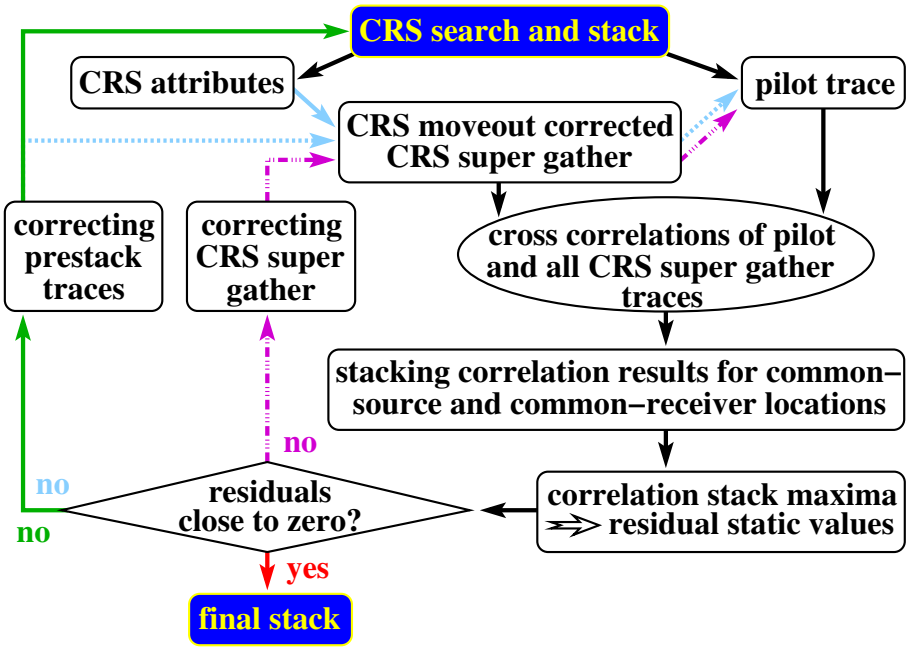

Figure 4: Flowchart for the iterative residual static correction by means of CRS attributes. Three alternatives are available for the second and further iterations: the CRS search for the attributes can be optionally performed again (solid green arrows). If not (see dashed and solid blue arrows), the pilot trace has to be recalculated from the CRS moveout corrected CRS super gather to take advantage of the enhancements of the previous iterations. A third option (dash-dotted purple arrows) can be used to directly correct the previously calculated CRS super gather with the obtained residual static values.

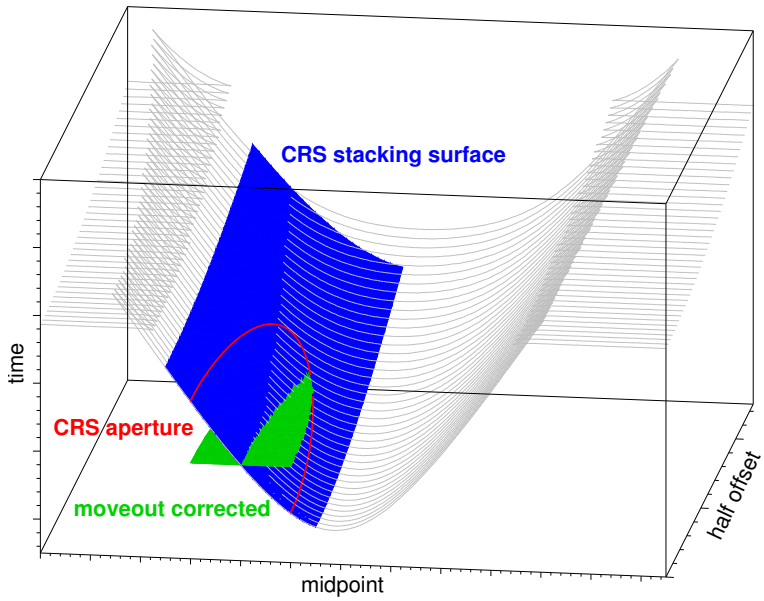

Figure 5: CRS moveout correction example for one time sample. The blue surface is the CRS stacking operator given by α, R_{NIP}, and R_{N}. With equation (2), the moveout can be subtracted which results in the flattened operator here shown as green horizontal plane at time t_0.

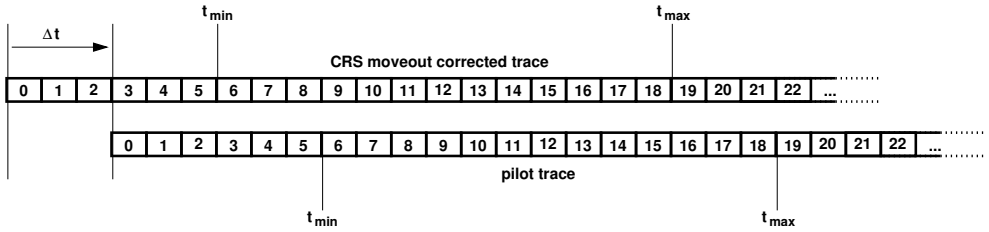

Figure 6: Cross correlation of a CRS moveout corrected trace and a pilot trace for a given time shift Δt.

This correction is performed for all t_0 given by each simulated ZO trace of the CRS stack. The result for one ZO trace is called CRS moveout corrected CRS super gather and contains all CRS moveout corrected prestack traces which lie inside the corresponding spatial CRS aperture (shown as red half-ellipse in Figure 5). Thus, the prestack traces are multiply contained in different CRS super gathers with different moveout corrections in each super gather.

Cross correlation

After the moveout correction has been applied, the traces are assumed to be misaligned by the residual statics for the source and for the receiver location. Thus, the cross correlation with the corresponding pilot trace should yield the total static shift for this trace. Then, the cross correlations are performed between every single moveout corrected trace of each CRS super gather and the corresponding trace of the simulated ZO section, i. e., the pilot trace. These correlations can also be weighted with the coherence values provided by the CRS stack to account for the reliability of every single sample. Additionally, the traces can be normalized before the correlation or the correlation results can be normalized before the correlation stack to balance their influence on the correlation stack. The normalization before cross correlation can be selected in the same way as for the coherence analysis of the CRS stack (here, we used the division by the envelope of its analytical signal). The normalization of the correlation results is realized by a division by its power. Afterwards, all correlation results that belong to the same source or receiver location are summed up. The resulting cross correlation stacks for each source or receiver location, respectively, are similar to cross correlating super-traces as proposed by Ronen and Claerbout (1985).

The main difference to CMP gather-based methods is that the correlation of the super-traces accounts for the subsurface structure because super-trace G of Figure 3 is a sequence of neighboring stacked traces and not of one stacked trace repeated multiple times. Super-trace F consists of all traces belonging to the same source or receiver location, respectively. The CRS stack accounts for the subsurface structure by means of the CRS attribute R_{N} which enters into the CRS moveout correction. R_{N} is the radius of curvature of the normal wave measured at the surface and can be associated with an hypothetical exploding reflector experiment.

The residual static value is assumed to be associated with the global maximum of the summed correlation results. However, the cross correlations are, in general, affected by a tapering effect. Figure 6 shows the cross correlation of the pilot trace with a CRS moveout corrected trace for a given time shift Δt. Only the part of a selected window from t_{min} to t_{max} should be correlated. In case of discrete cross correlation, the rest of the traces will be zeroed out. Thus, in this example only samples 9 to 18 from the CRS moveout corrected trace and samples 6 to 15 from the pilot trace will contribute to the correlation result. Nevertheless, the traces still contain data outside the selected window which can help to reduce the taper effect in the cross correlation. Therefore, we do not zero out the traces before the cross correlation to reduce the taper effect. In this example, it means that samples 6 to 21 from the CRS moveout corrected trace and samples 3 to 18 from the pilot trace are taken into account for the correlation.

Problems might occur at the boundary of the data set because there only few correlation results will contribute to source or receiver locations. Therefore, we implemented a threshold for the maximum correlation shift, i. e., a maximum residual static time shift. This threshold also reduces the likelihood of cycle skips. Furthermore, an additional threshold is introduced which handles the reliability of the estimated statics. As we count how much traces contribute to each source or receiver correlation stack (see Figure 7),

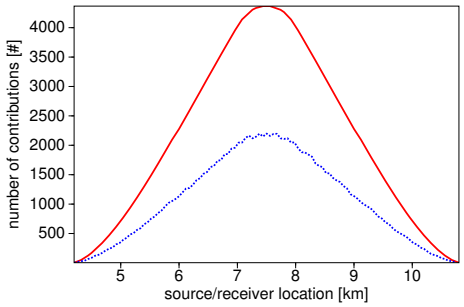

Figure 7: Example for the number of contributions to the cross correlation stacks for source (red solid line) and receiver (blue dotted line) locations from a split-spread acquisition geometry. The number of contributions depends on the size of the CRS aperture in midpoint and offset direction.

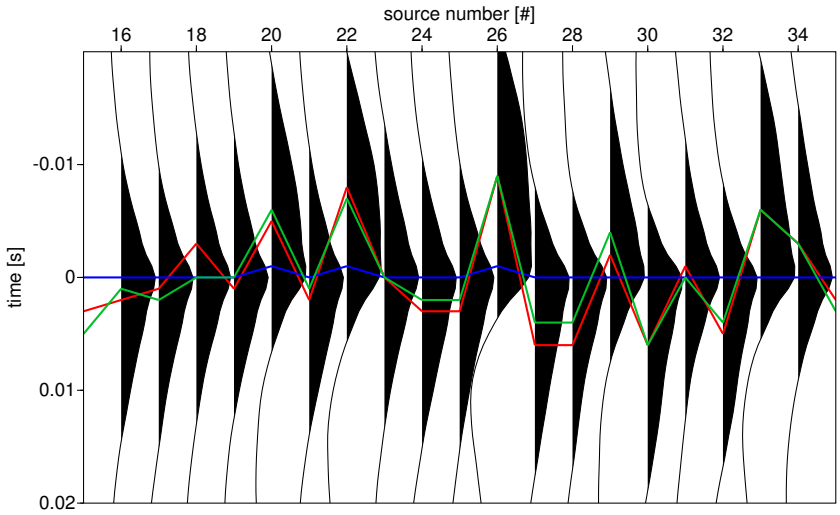

Figure 8: Example for asymmetrical correlation stacks. The red line displays the artificial time shifts which where added to a not too complex real data set. The blue line shows the estimated time shifts by picking the global maxima (almost zero for each location) and the green line shows the estimated time shifts using the center of the positive lobe around the global maxima (close to the red curve), both after the first iteration.

we introduced a minimum threshold for the number of contributions to each correlation stack. Thus, if the number of contributions is too low at the boundary of the data set or due to acquisition gaps, then the estimated static might not be reliable and will be omitted for the subsequent correction.

Estimation of residual statics

Finally, the residual static value have to be estimated from the cross correlation stacks. As mentioned before, the residual statics are usually assumed to be associated with the global maximum of the correlation results. From our tests, we have seen that this is not always the best choice as most global maxima are located at a zero time shift but with an asymmetrical positive area around it. Thus, we introduced another automatic picking algorithm instead of simply extracting the global maxima. Now, it is possible to define a minimum threshold which is a percentage of the global maximum or the local maximum closest to a zero time shift. Then, the center of the positive lobe defined by this threshold is used as the estimated time shift. Figure 8 shows an example of asymmetrical correlation results from a not too complex real data set. The blue line indicates the estimated time shifts using the global maximum and the green line displays the estimated time shift by using the center of the positive lobe. The red line indicates the artificially added time shifts. This example shows that the new automatic picking algorithm can help to strongly reduce the

required number of iterations (for this example: from 6-7 iterations down to 2-3 iterations).

Iteration

Once the residual static values are obtained from the cross correlation results, the prestack traces are time shifted with the corresponding total time shifts. The total time shift is simply the sum of the corresponding source and receiver static values of each prestack trace. If the CRS stack of these corrected prestack traces is not yet satisfactory, the entire procedure can be started again in two different ways with the previously corrected prestack traces or, alternatively, with the previously corrected CRS super gathers. The first possibility is to again perform the CRS search and all other steps (see solid green arrows in Figure 4). The second possibility omits the CRS search for the attributes (see dashed blue arrows in Figure 4). As the CRS search for the attributes is the most time consuming step of our method, it is attractive to omit this step. However, it might be dangerous to rely on the CRS attributes: if the time shifts between neighboring traces are too large, the CRS stack probably fails to detect actually contiguous events and the corresponding attributes. The third possibility is to use the obtained residual static values to directly correct the traces of the CRS super gathers. However, this approach is not surface-consistent as the static time shifts are applied to moveout corrected traces. Thus, the corresponding prestack traces are no longer shifted by a static time, every time sample of one trace has to be shifted by different times. As one prestack trace is multiply contained in the CRS super gathers but with different moveout corrections, the time shifts for each sample also depend on the currently considered midpoint and its associated moveout correction. Some results for the second and third possibility as well as combinations of all three possibilities can be found in Ewig (2003).

REAL DATA EXAMPLE

The reflection seismic data used for the following case study were acquired by an energy resource company. To get a detailed knowledge of the subsurface structure in the area of interest, data were acquired along two parallel lines denoted as A and B. On each line, about 240 geophone groups were laid out in a fixed-spread geometry with a group spacing of 50 m. The source signal was a linear upsweep from 12 Hz to 100 Hz of 10 s duration, generated by three vibrators. The source spacing was 50 m and the temporal sampling interval was 2 ms. For the examples shown in this paper, data from line A are used and due to the small changes in elevation, we did not consider the topography during the application of CRS to this data set.

A contractor applied a standard preprocessing and imaging sequence to the data sets, the latter consisting of normal moveout (NMO) correction/dip moveout (DMO) correction/stack, conventional residual static correction, and further more steps like migration. We were kindly provided with their results before and after conventional residual static correction. The ZO section of the CRS stack applied to the data set before any residual static correction is shown in Figure 9(a). The stacked section contains several reflection events well imaged, but there are also areas of poor image quality. Figure 9(b) shows the ZO section of the CRS stack applied to the data set after a conventional residual static correction has been applied. The difference of these two plots is obvious as the S/N ratio has increased for almost all reflection events after the application of conventional residual static correction. In comparison to Figure 9(b), Figure 10(a) shows the ZO section of the optimized CRS stack after we have applied three iterations of our new approach of residual static correction to the original data set with no residual static correction of the contractor. The arrows indicate two areas where we improved the continuity of reflection events. And also at the left border, Figure 10(a) shows some improvements on reflector continuity compared to Figure 9(b). The estimated residual statics are displayed in Figure 11(a) for the source locations and in Figure 11(b) for the receiver locations. The green solid curves are the results after three iterations of our CRS-based approach and the red/blue dotted lines are the conventional results. One can observe areas with different levels of correlation. This can be also observed in the stacked sections. Thus, we think that each of the residual static corrections provided one solution to the ambiguous problem of residual statics.

We also applied our new approach directly to the provided data set with the conventional residual static correction applied to see whether there remained some residual statics in this data set. We performed two iterations with a new CRS attribute search in each step. The ZO section of the optimized CRS stack after these iterations is shown in Figure 10(b). The estimated residual statics of the second iteration did not yet

vanish completely for each source or receiver location (see Figure 12(a) and Figure 12(b), respectively). Nevertheless, we stopped to iterate further as the changes are expected to be minimal. Figure 12(a) and Figure 12(b) display the obtained time shifts after the second iteration. As expected, they are smaller and there are also areas where no further changes appeared (zero time shifts). The stacked section shows some small changes which in some areas increased or decreased the reflection event continuity or the S/N ratio. Thus, it is up to the interpreter to decide which result is easier to interpret or, even more important, closer to reality. However, we presented here only the stacked ZO sections of the CRS stack results but also the sections of the CRS attributes have to be taken into account for a more sophisticated comparison.

CONCLUSIONS

Residual static correction methods are, in general, based on cross correlations. We showed that the CRS stack method can help to derive the residual statics. The advantages of the CRS stack method, i. e., the improved S/N ratio and the additional information about the subsurface by the CRS attributes compared to, e. g., NMO/DMO/stack, is integrated into our new approach. The CRS stack method fits entire surfaces to reflection events which is essential for a moveout correction within a spatial aperture. Also, the traces of the simulated ZO section are better suited as pilot traces than conventional CMP stacked traces because of the large spatial aperture. Our new approach combines the conventional methods (cross correlation, picking of correlation maxima) with the advantages of the CRS stack. Here, the large spatial aperture of the CRS stack takes far more traces into account than just correlating within CMP gathers. Furthermore, the coherence of the CRS stack serves as a reliability measure and weight factor for the traces during the cross correlation.

With the example of this real data set, we demonstrated that our new approach is able to estimate residual statics in order to enhance the simulated ZO section after this correction (see Figure 10(a)). Additionally, our approach can also be applied to data sets already corrected by residual statics to further enhance the ZO section (see Figure 10(b)). Despite of simply picking the global maximum of the summed cross correlation results, we have implemented picking of the center of positive lobes in the correlation results which decreases the number of required iterations compared to pick global maxima.

PUBLICATIONS

Detailed results on synthetic and a not too complex real data set were published by Ewig (2003). Extended Abstracts on the theoretical background are also available from Koglin and Ewig (2003a) and Koglin and Ewig (2003b).

ACKNOWLEDGMENTS

This work was kindly supported by the sponsors of the *Wave Inversion Technology (WIT) Consortium*, Karlsruhe, Germany. Additional thanks go to Dr. Franz Kirchheimer for his ideas and suggestions and to Dr. Jürgen Mann for his help in implementing the new approach into the CRS code.

REFERENCES

Cox, M. (1974). *Static Correction for Seismic Reflection Surveys*. Society of Exploration Geophysicists.

Ewig, E. (2003). Theory and application of residual static correction by means of CRS attributes. Master's thesis, Karlsruhe University, Germany.

Koglin, I. and Ewig, E. (2003a). Residual static correction by means of CRS attributes. In *Expanded Abstracts*, pages 1889 – 1892. 73rd Annual Internat. Mtg., Soc. Expl. Geophys. Session SP 1.4.

Koglin, I. and Ewig, E. (2003b). Residual Static Correction by Means of Kinematic Wavefield Attributes. In *Extended Abstracts*. 65th Annual Internat. Mtg., Eur. Assn. Geosci. Eng. Session D18.

Mann, J. (2002). *Extensions and Applications of the Common-Reflection-Surface Stack Method*. Logos Verlag, Berlin.

Mann, J., Jäger, R., Müller, T., Höcht, G., and Hubral, P. (1999). Common-reflection-surface stack – a real data example. *J. Appl. Geoph.*, 42(3,4):301–318.

Marsden, D. (1993). Static corrections—a review. *The Leading Edge*, 12(1):43 – 49.

Ronen, J. and Claerbout, J. F. (1985). Surface-consistent residual statics estimation by stack-power maximization. *Geophysics*, 50(12):2759 – 2767.

Taner, M. T., Koehler, F., and Alhilali, K. A. (1974). Estimation and correction of near-surface anomalies. *Geophysics*, 39(4):441 – 463.

Trappe, H., Gierse, G., and Pruessmann, J. (2001). Case studies show potential of Common Reflection Surface stack – structural resolution in the time domain beyond the conventional NMO/DMO stack. *First Break*, 19(11):625 – 633.

Wiggins, R. A., Larner, K. L., and Wisecup, R. D. (1976). Residual static analysis as a general linear inverse problem. *Geophysics*, 41(5):922 – 938.

Zhang, Y. (2003). *Common-Reflection-Surface Stack and the Handling of Top Surface Topography*. Logos Verlag, Berlin.

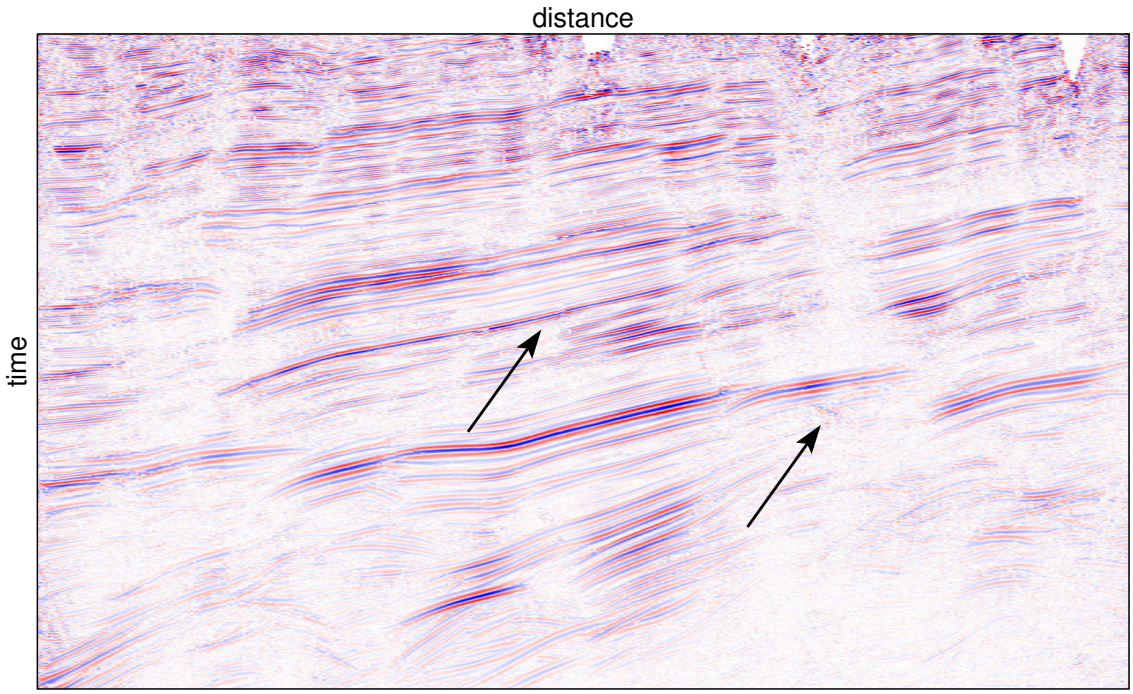

(a) before any residual static correction

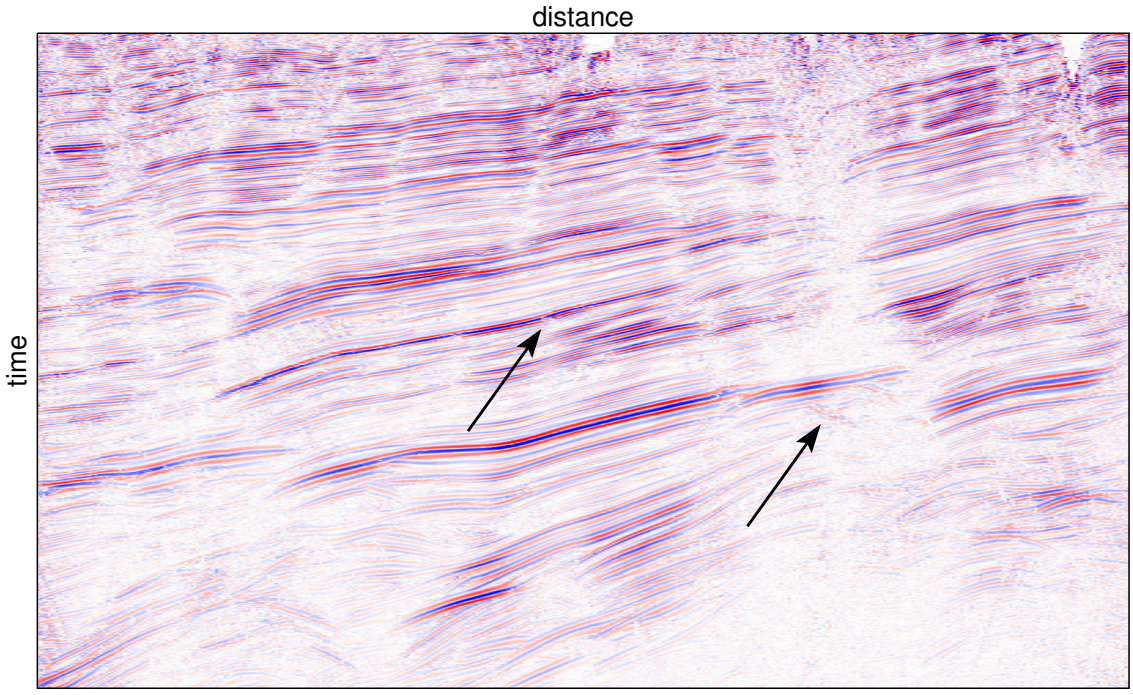

(b) after a conventional residual static correction method has been applied

Figure 9: Simulated ZO sections of the optimized CRS stack.

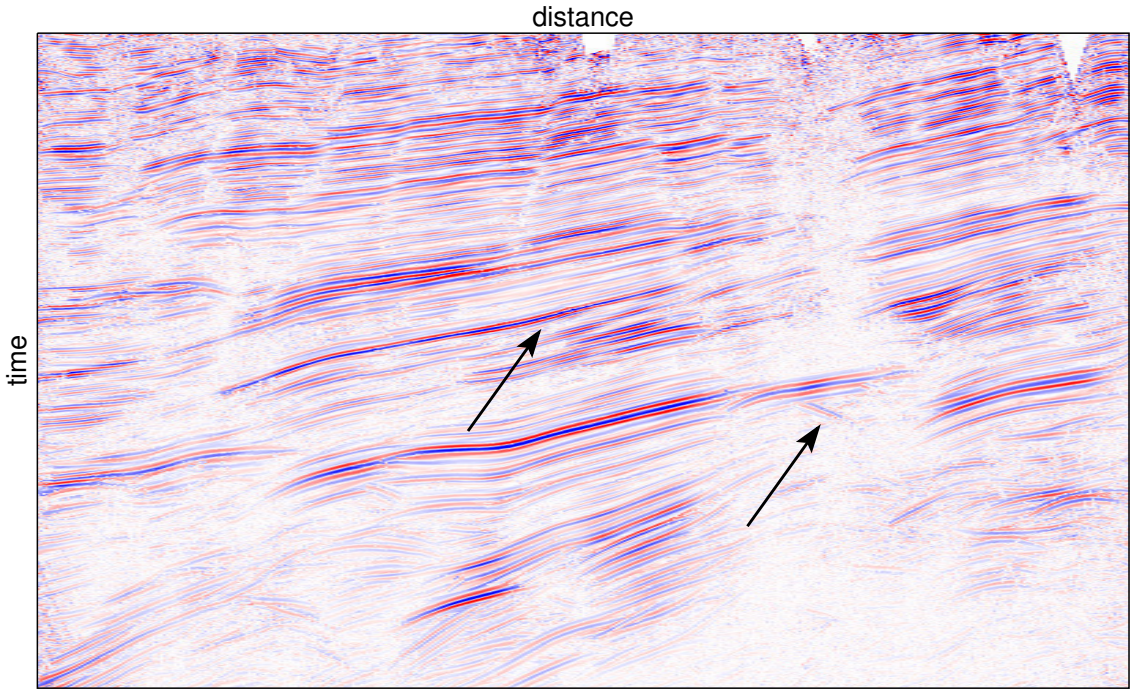

(a) after three iterations of our residual static correction method with a new CRS attribute search in each step

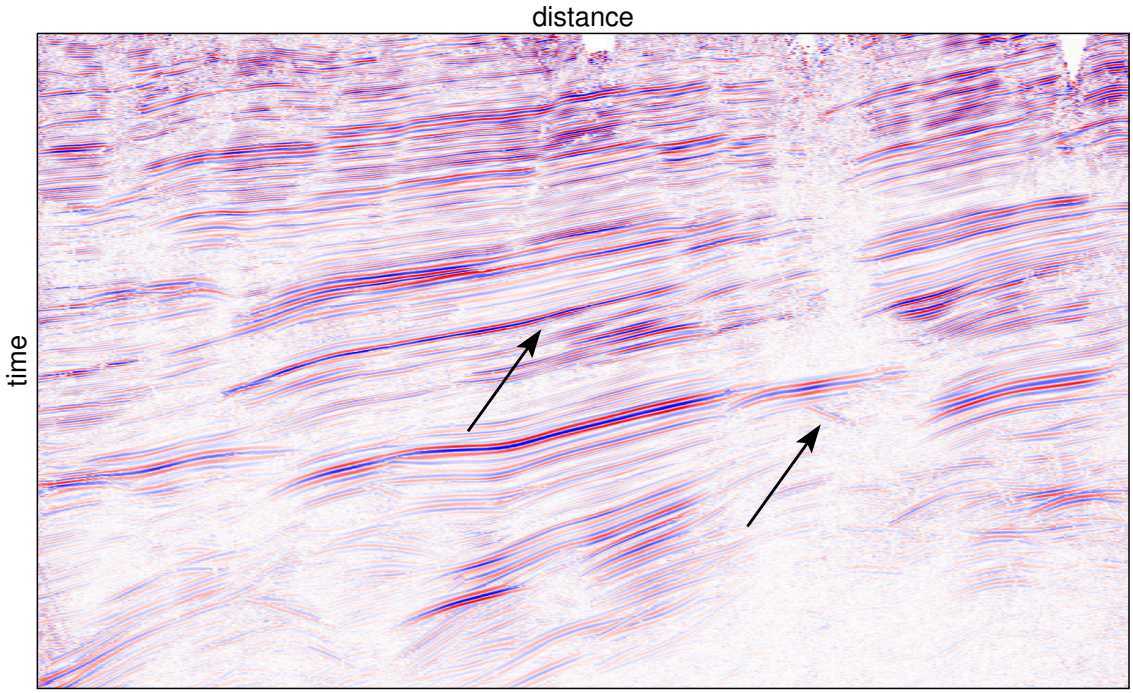

(b) after conventional residual static correction provided by a contractor and two iterations of our residual static correction method with a new CRS attribute search in each step

Figure 10: Simulated ZO sections of the optimized CRS stack.

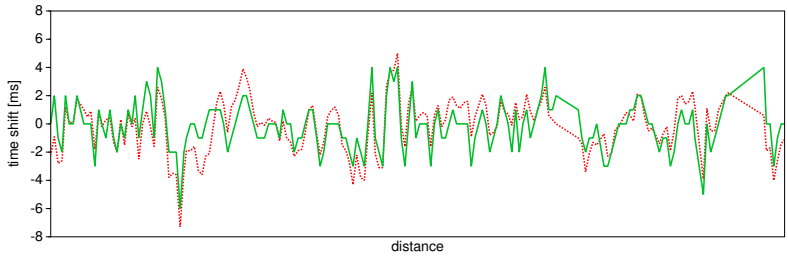

(a) source time shifts

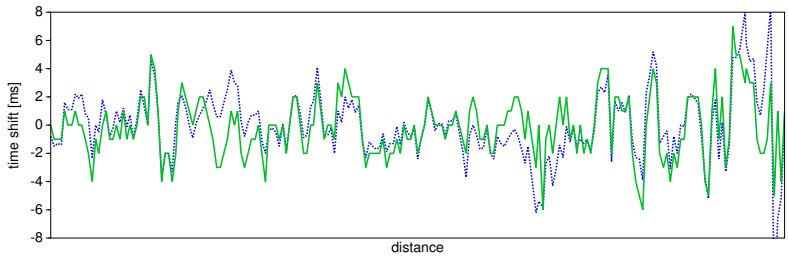

(b) receiver time shifts

Figure 11: Obtained time shifts as green solid lines after three iterations applied to the data set before any residual static correction compared with the conventional residual statics displayed as dotted lines in red for source locations and in blue for receiver locations, respectively.

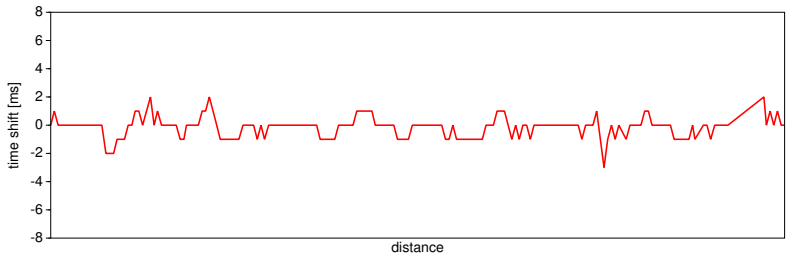

(a) source time shifts

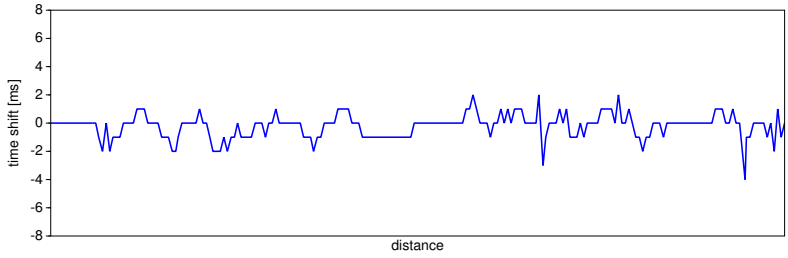

(b) receiver time shifts

Figure 12: Obtained time shifts after the second iteration applied to the data set with conventional residual static correction applied.